8TH EUROPEAN CONFERENCE FOR AERONAUTICS AND AEROSPACE SCIENCES (EUCASS)

DOI: ADD DOINUMBER HERE

Low-order Modeling of Combustion Instability Applied to Cryogenic Propellants

Simone D'Alessandro°†, Gabriele Fedeli°, Federica Tonti⋆, Justin S. Hardi⋆, Michael Oschwald⋆, Bernardo Favini° and Francesco Nasuti°
°Sapienza, University of Rome
Via Eudossiana 18, 00184, Rome, Italy
⋆German Aerospace Center (DLR)–Institute of Space Propulsion
Lampoldshausen, Hardthausen, 74239, Germany
simone.dalessandro@uniroma1.it · fedeli.1558585@studenti.uniroma1.it
federica.tonti@dlr.de · justin.hardi@dlr.de · michael.oschwald@dlr.de
bernardo.favini@uniroma1.it · francesco.nasuti@uniroma1.it
†Corresponding author

Abstract

Combustion instability is a major threat to be dealt with during the design and development phase of new liquid rocket engines. If unpredicted, its onset easily yields to thermal or mechanical failure of the engine and of the mission as well. The present work focuses on the low-order modeling of combustion instability. In particular, a recently introduced response function formulation is reported and applied. Its novelty lies in the indirect link between acoustics and unsteady heat release, which passes through the modeling of the shear coaxial injector dynamics. Such injector is assumed to be capable of cyclically accumulating and releasing propellant vortexes where the mixing takes place. Such model is then applied to two different test-cases, namely one fed by gaseous propellant, i.e. the CVRC test-case, while the other by supercritical fluids, namely the BKD test-case. Results show how the CVRC instability features are well reproduced, while several model improvements are needed for the BKD.

1. Introduction

Combustion instability occurs in liquid rocket engines as a result of the coupling between different phenomena, like hydrodynamics, acoustics and combustion, with detrimental effects on the engine performance or yielding even to the failure of the system.[21]

In fact, severe pressure oscillation can be observed, their amplitude can reach the order of magnitude of mean chamber pressure, yielding to unexpected dynamic and thermal loads. High frequency instability is hard to be predicted, due to the number of phenomena that might give contribution in its sustainment. In particular, liquid rocket engines are complex systems in which the characteristics of propellant injection plays a fundamental role. In this sense, phenomena such as atomization, vaporization and mixing can be part of the instability onset. The wide range of time and length scales that characterize the above mentioned phenomena together with the chamber acoustics and combustion, governed by chemical kinetics, makes the investigation even more challenging.

The research in this area is based on the combined use of experiments and a hierarchy of modeling approaches,[30] from high-fidelity simulation to low-order models. High-fidelity computations have been widely used for research purposes, in order to get insights in the phenomenon as supporting tool for the experiments.[1–3,14–17,27,31–34] Although providing a huge amount of details necessary for understanding of phenomena and knowledge enhancement, the high-fidelity computations must be supported by reduction methods to identify the governing design parameters. Moreover, such approach cannot be considered as an option for supporting the design phase of a new engine due to the extreme computational effort required to study a single engine configuration. For these reasons, the development of reliable low-order models is crucial. Low-order models are usually characterized by some simplifying assumptions for the flow modeling that, on one side, are capable of reducing the required computational effort, but on the other, lead to the necessary introduction of suitable response functions. The response function is a term in the governing equations capable of modeling the coupling between acoustics and combustion.

DOI: 10.13009/EUCASS2019-617

Several low-order models have been proposed in the literature. Among those focusing on nonlinear analysis, Culick and Yang[5] proposed a method that has been applied later by Portillo et al.[24] for determining the growth rate and the resulting amplitude of pressure oscillations at limit cycle. In the same area of investigation of nonlinear regime, Sirignano and Popov[28] and Popov et al.,[23] proposed a model devoted to the investigation of transverse instability. Last but not least, Smith et al.,[30] used quasi-1D Euler equations for the investigation of longitudinal instability in single element combustors. All of them are based on a suitable response function.

The final aim of low-order model is to get quick analyses, better understanding and first evaluation of chamber behavior, by suitably modeling the main driving mechanisms of thermoacoustic combustion instability. Therefore, the identification of the response function is the core aspect of the above mentioned low-order models, as it should be capable of retaining the essential physics which governs the coupling occurring in unstable test cases. The process of response function derivation is usually based on the analysis of experimental data or high-fidelity simulation results. The n-τ function, based on Crocco's time lag theory,[4] is a possible option for response function selection, which has been widely used with suitable calibration (see for instance Refs. 6, 8, 24, 40). Different models can be found in the literature, each one related to a particular coupling mechanism. Some examples are the response function by Matveev,[19] particularly suitable for dump combustors where vortex shedding occurs, and the response function proposed by Culick and Yang,[5] based on modal development, and the simplified combustion model proposed in Refs. 23, 28 and used for the study of transverse instability.

In the present work, the use of a novel formulation for the response function introduced in Frezzotti et al.[7] is extended to a different application. The formulation is based on the modeling of the response of propellants injection to pressure oscillations, rather than rely on the more common assumption of linking heat release directly to pressure oscillations. Such an approach is inspired by several experimental test cases where longitudinal and transverse instability observed in the combustion chamber are related to a longitudinal dynamics taking place in the injectors which shows fuel accumulation and release.[11,15,35] The response function formulation is implemented in a one-dimensional Eulerian solver which allows for the simulation of longitudinal combustion instability.

The paper is organized as follows. First of all, the numerical model is presented. Then, after introducing the test cases and the selected geometries, results of the successful application of such model to a gaseous propellant system are presented. After that, ongoing developments on the application of the model to a supercritical propellant system are shown. Finally, concluding remarks are reported.

2. Numerical Model

The numerical model has been introduced in Frezzotti et al.[7] and addresses the study of longitudinal combustion instabilities in single element rocket combustors. A one-dimensional modeling is considered, which is referred to as "quasi-1D" to emphasize that cross-section area changes are allowed as a function of the single spatial variable. The thorough study of the single element dynamics is considered as a mandatory step towards the modeling and study of multidimensional problems.

The problem is approached using multi-species quasi-1D Euler equations. The minimum number of species is considered, which are the fuel, the oxidizer and the combustion products mixtures, the latter being the result of equilibrium reaction of fuel and oxidizer at stoichiometric proportion. Therefore, the governing equations are:

$$(\rho A)_t + (\rho u A)_x = \dot{\omega}_{f1} \tag{1}$$

$$(\rho A Y_{ox})_t + (\rho u A Y_{ox})_x = -\dot{\omega}_{ox} \tag{2}$$

$$\left(\rho A Y_f\right)_t + \left(\rho u A Y_f\right)_x = \dot{\omega}_{f1} - \dot{\omega}_{f2} \tag{3}$$

$$(\rho u A)_t + \left[\left(\rho u^2 + p\right) A\right]_x - p A_x = u \dot{\omega}_{f1} \tag{4}$$

$$(\rho e_0 A)_t + (\rho u h_0 A)_x = \dot{\omega}_{f1} h_{0f} + \eta_c (\dot{\omega}_{ox}\, \Delta h^o_{f,ox} + \dot{\omega}_{f2}\, \Delta h^o_{f,f} - \dot{\omega}_p\, \Delta h^o_{f,p}) \tag{5}$$

where ρ, u, p, Y_{ox} and Y_f are density, velocity, pressure, oxidizer and fuel mass fraction; e_0 and h_0 are the specific total internal energy and total enthalpy which include the kinetic energy, $u^2/2$, and are linked to pressure and density via the perfect gas law. Source terms on the right hand side represent the contribution of mass addition and combustion. In particular, $\Delta h^0_{f,ox}$, $\Delta h^0_{f,f}$ and $\Delta h^o_{f,p}$ are the formation enthalpies of the three species; $\dot{\omega}_{ox}$ and $\dot{\omega}_{f2}$ are the rate of consumption of oxidizer and fuel per unit length, respectively, which are positive values associated to combustion and providing products at the positive rate

$$\dot{\omega}_p = \dot{\omega}_{ox} + \dot{\omega}_{f2} \tag{6}$$

DOI: 10.13009/EUCASS2019-617

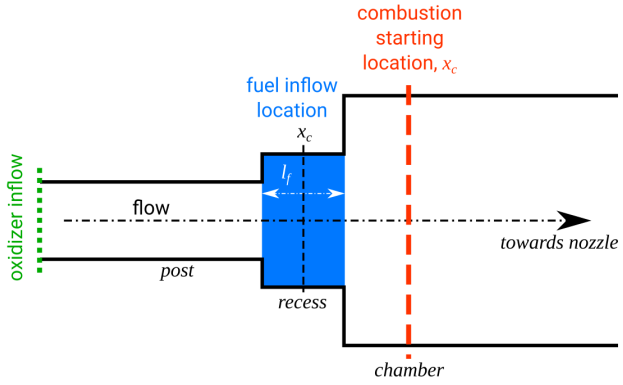

Figure 1: Fuel addition zone and combustion starting location detail.[7]

while $\dot{\omega}_{f1}$ is the term of mass addition due to fuel injection. Finally, A is the cross-section area and η_c is the combustion efficiency which multiplies the heat of reaction.

The thermodynamic properties of each species are computed using CEA chemical equilibrium database.[20] Oxidizer is introduced at the left boundary, where oxidizer mass flow rate and stagnation temperature are considered as known.

Fuel is introduced in a length l_f centered at the abscissa x_r, which is representative of the recess position, as shown in Figure 1. For this reason the fuel mass flow rate source term at steady state is cast as

$$\dot{\omega}_{f1} = \begin{cases} \dfrac{\dot{m}_f}{l_f} & \text{for} \quad x_r - l_f/2 < x < x_r + l_f/2 \\ 0 & \text{elsewhere} \end{cases} \tag{7}$$

Similarly to fuel addition, combustion is modeled identifying a region where combustion reaction occurs. As shown in Figure 1, a location x_c is identified where the combustion reaction is allowed to start, downstream of the dump plane.

Combustion mechanism is modeled as a first order reaction between fuel and oxidizer. Fuel consumption is taken as proportional to fuel and oxidizer mass fraction according to

$$\dot{\omega}_{f2} = \begin{cases} \dfrac{\dot{m} Y_f Y_{ox}}{l_c} e^{-T/T_r} & \text{for} \quad x > x_c \\ 0 & \text{elsewhere} \end{cases} \tag{8}$$

while the oxidizer depletion rate, as mentioned, assumes that it reacts with fuel at stoichiometric proportion

$$\dot{\omega}_{ox} = OF_{st}\, \dot{\omega}_{f2} \tag{9}$$

to form products at the rate $\dot{\omega}_p$ expressed in Eq. (6). Based on Eq. (8), the reference length l_c determines the width of the main reaction region and the reference temperature T_r determines the shape of the heat release curve. In fact, the term in parentheses at right hand side of Eq. (5) represents the heat released due to propellant conversion in reaction products and it is positive according to typical negative values of $\Delta h^o_{f,p}$ and positive or zero values of $\Delta h^0_{f,f}$ and $\Delta h^0_{f,ox}$. A further parameter to control the amount of heat effectively released during combustion and absorbed by the gases is the mentioned combustion efficiency η_c.

2.1 The response function

The most commonly used approach to model the coupling between pressure oscillations and heat release, which drives thermoacoustic combustion instabilities, is based on direct relationships between them.[7] The followed approach to model such coupling is something different. In fact, it has been shown in the literature that instabilities develop from the coupling between the chamber and the injection system dynamics, and in particular from the strong pressure waves causing cyclic fluctuation of the propellant flow. Such behavior has been highlighted for both longitudinal and transverse instabilities.[11,15,35] More specifically, CFD simulations have shown that the instability in coaxial injectors can be driven by one of the propellants accumulation and release process.[15]

The response function is developed on the propellant addition, rather than on the heat release, with the aim of keeping as much physics as possible in the low-order model. In the following, for simplicity the response function

DOI: 10.13009/EUCASS2019-617

is applied to fuel, keeping in mind that it can also be applied to the oxidizer. Fuel mass flow rate injection model allows for its accumulation at the injection position and subsequent release in the flow field depending on the local flow conditions. Such dynamics allows for the fuel to be injected at higher or lower rate than its steady-state value. The basic criteria followed to build up the response function model are: fuel accumulation and release are based on pressure fluctuations (null for null fluctuations); the maximum quantity of fuel that can be accumulated at each time step equals the fuel mass flow rate; and the fuel released cannot exceed the runtime-integrated amount of available fuel mass.

The approach is implemented embedding the response function in the source term of fuel continuity equation. The instantaneous mass flow rate $\dot{m}_f$ appearing in Eq. (7) is expressed as

$$\dot{m}_f = \dot{m}_{f,0} + \dot{m}'_f \tag{10}$$

where $\dot{m}_{f,0}$ is the nominal fuel mass flow rate and $\dot{m}'_f$ is the fluctuation of mass flow rate generated by unsteady pressure.

The mass flow rate oscillation is modeled as depending on the normalized local pressure oscillation according to an exponential law by the following expression

$$\dot{m}'_f = \min\left[\hat{\dot{m}}'_f\,,\ \frac{m_{f,acc}}{\Delta t}\right], \qquad \text{where} \quad \hat{\dot{m}}'_f = \dot{m}_{f,0}\left(e^{-\sigma\,(p'/p_0)} - 1\right) \tag{11}$$

where σ is a calibration parameter, p_0 is a reference pressure, sampled just downstream of the mass addition zone at a position x_p, p' represents the fluctuation in time with respect to the reference value, i.e. $p' = p'(t) = p(t) - p_0$, and Δt is the integration timestep.

In case the fluctuating pressure p' becomes positive, $\hat{\dot{m}}'_f$ turns negative and the fuel mass flow rate injected in the core flow decreases from the nominal value. Assuming that the actual overall fuel mass flow rate $\dot{m}_{f,0}$ is constant, the missing amount is accumulated in a vortex, assumed to live in the recess, where the shear mixing occurs. Therefore, the extra mass of fuel available $m_{f,acc}$ can be defined as:

$$m_{f,acc} = \int_0^t \dot{m}'_f\, dt' \tag{12}$$

where t is a generic time during integration.

On the other hand, if the local pressure decreases, $\dot{m}'_f$ becomes positive and such amount of fuel mass is partly or completely released, according to Eq. (11), increasing the local fuel mass flow rate.

The exponential behavior is arbitrarily selected here as a suitable function to have a smooth asymptotic behavior to zero when $p' > 0$. The behavior of the instantaneously released fuel mass flow rate is shown in Figure 2 for normalized pressure fluctuations in the ±30% range. It has to be noticed that abrupt variations of instantaneous fuel mass flow rate in time have to be expected in the range of negative values of p'. In fact, if the pressure decreases in time, the mass flow rate increases but when all the accumulated mass has been released, the mass flow rate value suddenly reduces to the nominal value. Such behavior can be deduced from Eq. (11), where $\dot{m}'_f$ becomes zero if the fuel mass $m_{f,acc}$ is zero.

Since the propellant mass flow rate varies with time, a different amount of it is burnt through the combustion region yielding to a variable heat release rate in time, producing in turn new pressure fluctuations which close the thermoacoustic instability feedback loop.

3. Test-cases

Two test-cases are dealt with within the scope of this work. Sorting them by simplicity, the first analyzed test-case is the Continuously Variable Resonance Combustor (CVRC) experiment, realized and installed at Purdue University with the objective of investigating the effect of oxidizer post length on instability.[39] Such test-case is operated with warm gaseous propellant, whose temperature does not go below the ambient temperature. Operating at such conditions, the ideal gas assumption, which has been taken into account in the model, holds. This test case was already studied and discussed in detail in Frezzotti et al.[7] and is reported here for the sake of completeness.

The latter selected test-case is the Research Combustor D (BKD) system, which is installed and tested at DLR in Lampoldshausen, Germany.[11] Such rocket combustor is affected by transverse combustion instability. For the purpose of better understanding its behavior, the quasi-1D model is used for the study of one of its injectors at representative thermodynamic and acoustic condition of the BKD chamber. BKD is operated with supercritical propellant and this aspect represents an additional complication to deal with in the low-order modeling. The study of this latter test case consitutes the main goal of the present study.

DOI: 10.13009/EUCASS2019-617

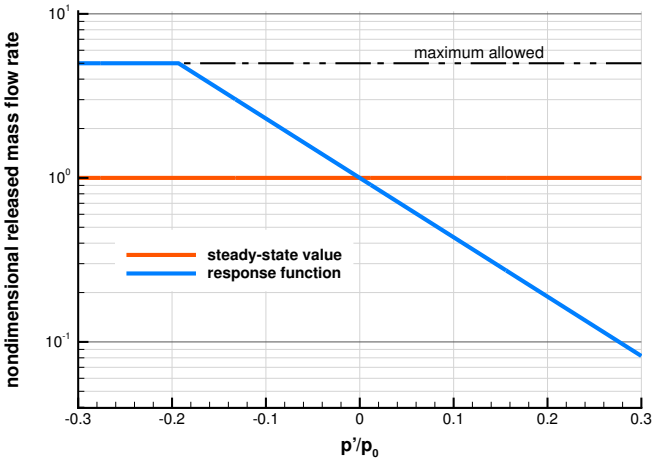

Figure 2: Fuel mass flow rate release curve compared to the nominal value.[7]

3.1 CVRC test-case

CVRC propellants are hydrogen peroxide, dissociated in water and oxygen on a catalyst bed, and methane, injected through a single coaxial injector. Both propellant are in gaseous phase. This single element combustor has been widely studied through a number of experiments and simulations.[6,8,9,14–16,22,25,26,29,31,32,37–39]

The characteristic feature of CVRC is the presence of a translating shaft capable of continuously varying the length of the oxidizer post. Changing the geometry, transition from stability to instability and vice versa is observed. In particular, the region of short and long post tend to be stable while the intermediate lengths lead to unstable conditions. As shown from results of test campaign in Yu et al.,[39] the transition in the region of short post is more neat, while for the long post configuration a range of possible transition lengths is observed. In the present study three fixed oxidizer post length configurations are considered, one in the short post transition region, one in the fully unstable region and one in the long post transition region. The experimental data for comparison with simulations are taken from the literature,[36] as well as average operating conditions[15] which are summarized in Table 1.

The procedure to obtain the unstable behavior follows the approach considered in previous works.[6,8,30] It includes a first step where a simulation aimed to get a reference steady state flow field is carried out. A steady state solution is easily obtained numerically with the response function turned off. Then, as a second step, the response function is activated after some noise has been introduced for a short time to trigger the possible thermoacoustic coupling.

The steady state analysis is useful to verify the capability of the numerical model to reproduce the main features of the combustor. According to the model the steady-state chamber pressure value obtained by quasi-1D simulations is the one corresponding to the value that can be obtained calculating the characteristic velocity at equilibrium for the mixture given in Table 1. This results in a value of $c^* = 1534$ m/s, slightly lower than the value of 1563 m/s that can be deduced from Yu et al.[39] and for the given throat diameter, a consequent value of chamber pressure of $p_c = 1.570$ MPa, which is slightly lower than the declared nominal 1.586 MPa. This value is independent of the length of the oxidizer post as it assumes ideal burning in the combustor. Compared to average values from experiments at stable and unstable operations, this pressure value is higher, as expected, because of combustion inefficiencies and possible heat losses[9,15] have not been taken into account. Considering data reported in Yu et al.[39] for the stable behavior, a chamber pressure decreasing from about 1.450 MPa is found, indicating a reasonable initial value of about 93% combustion efficiency. Lower average pressure values are measured during experiments which are only partially explained by heat losses, as they should decrease as the chamber walls are heated during time. Another possible explanation comes from the rough or unstable operation which would highlight a lower average combustion efficiency. Accordingly, it is known from the literature that if one considers a full combustion of reactants in the CVRC, the resulting chamber longitudinal acoustic frequencies are significantly higher than those found experimentally.[6,8,15,25,26]

To analyze the role of combustion efficiency the value of η_c in Eq. (5) has been changed in order to verify if a better match with the experimental average pressure reported in Yu et al.[39] would be obtained. A comparison of pressure and first longitudinal frequency evaluated with the selected combustion efficiencies is reported in Table 2, for the three analyzed test cases. Note that here the numerical frequencies are identified introducing a small amplitude

DOI: 10.13009/EUCASS2019-617

Table 1: CVRC geometrical data and operating conditions.[15,36]

Parameter	Value
Fuel Mass Flow Rate, kg/s	0.027
Fuel Temperature, K	300
Oxidizer Mass Flow Rate, kg/s	0.320
Oxidizer Temperature, K	1030
Oxidizer Mass Fraction H_2O, %	57.6
Oxidizer Mass Fraction O_2, %	42.4
Equivalence Ratio	0.8
Throat diameter, cm	2.080
Combustor length, cm	38.1
Combustor diameter, cm	4.500
Recess diameter, cm	2.306
Recess length, cm	1.01
Oxidizer post diameter, cm	2.047
Oxidizer post length (Long), l_{op}, cm	19.05
Oxidizer post length (Medium), l_{op}, cm	12.97
Oxidizer post length (Short), l_{op}, cm	8.89

Table 2: Comparison between numerical[7] and experimental[39] average pressure and first longitudinal frequency of CVRC. Numerical frequencies are obtained in regime of small amplitude perturbations.[7]

	l_{op} = 8.89 cm		l_{op} = 13.97 cm		l_{op} = 19.05 cm	
	Exp	Q-1D	Exp	Q-1D	Exp	Q-1D
η_c, %	—	80	—	78	—	93
p, MPa	1.40	1.40	1.36	1.38	1.45	1.47
f_1, Hz	1379	1750	1324	1395	1260	1350

DOI: 10.13009/EUCASS2019-617

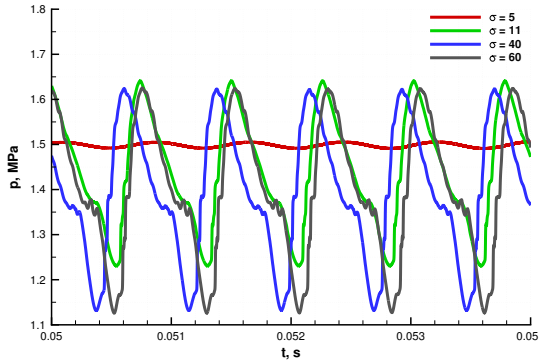

Figure 3: Parametric analysis on the σ parameter for the test-case with l_{op} = 19.05 cm.[7]

broadband disturbance on the oxidizer mass flow rate, assuming null response function.

Results shows that frequencies are still higher than experimental but also show that pressure and thus combustion efficiency is minimum at the most unstable operation, so the interesting consideration that can be drawn from the present analysis is that results show that during unstable operation of CVRC significant combustion inefficiency occurs.

3.1.1 Unsteady analyses results

In order to carry out the unsteady simulations, the reference pressure p_0 needs to be defined. In the present analysis it is considered as the average pressure experimentally measured during limit cycle and reported for each test-case (i.e. oxidizer post length) in Table 2.

At first instance, the combustion inefficiency needed to match experimental data in the steady state analysis has been attributed to the fact that average data are considered during rough or unstable operation, rather than actual steady-state measures, which is because smooth steady-state data are obviously not available. Therefore, if such an inefficiency comes from averaging the unsteady behavior, it has to be found as a result of the unsteady analysis. For this reason 100% efficiency (or $\eta_c = 1$) has been assumed for the unsteady analyses.

The only free parameter left in the model is the response function calibration parameter σ. For this reason, a sensitivity analysis to this parameter has been carried out for each configuration. Figure 3 shows the σ sensitivity analysis carried out for the test-case having l_{op} = 19.05 cm. The figure shows the pressure trend sampled at the step as a function of time, for different values of σ. It is quite clear that above a certain threshold value, once the unstable conditions have been obtained, the effect that such parameter has on the solution is not significant: even if the shape of the signal changes slightly, its amplitude, frequency and overall shape remain unchanged. Sensitivity analyses on the test-cases having l_{op} = 13.97 cm and l_{op} = 8.89 cm are not shown since they provide analogous results. Therefore, a suitable value for σ is chosen for each configuration above the mentioned threshold.

Results of the unstable simulations for each of the three geometrical configurations are shown in Figure 4. Pressure traces sampled at the backstep as a function of time are compared to the experimental paths available in the literarture.[25,31]

In each analyzed geometrical configuration it is possible to recover the global system behavior (rough combustion or instability). In particular, for the test-case having l_{op} = 13.97 cm (medium) unstable behavior is observed, in agreement with the experiments. The test-case with l_{op} = 8.89 cm (shorter) shows pressure oscillations close to the instability limit according with the experiments, while for the case l_{op} = 19.05 cm (longer), experimentally characterized by both stable and unstable operative conditions, the unstable load point is well reproduced. The characteristic frequencies at limit cycle are summarized in Table 3. The longer configuration simulation is able to reproduce both amplitude and frequency of the experimental pressure signal. The medium length configuration shows good agreement in frequency but its amplitude is lower ($\sim$ 50%), while the shorter geometry lacks in frequency ($\sim$ 20%) but reproduces quite well the amplitude of the pressure trace of the engine. An important aspect that has to be remarked is that in each simulation the shape of the pressure signal is reproduced with significant agreement. This means that the main gasdynamic and thermal events taking place inside the engine are caught by the model, even if the formulation is strongly simplified.

DOI: 10.13009/EUCASS2019-617

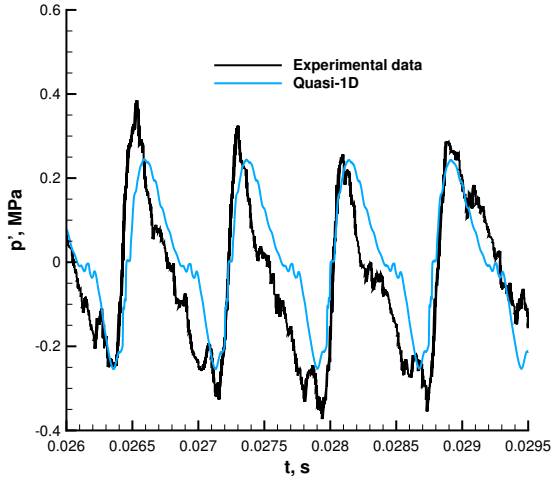

(a) l_{op} = 19.05 cm.

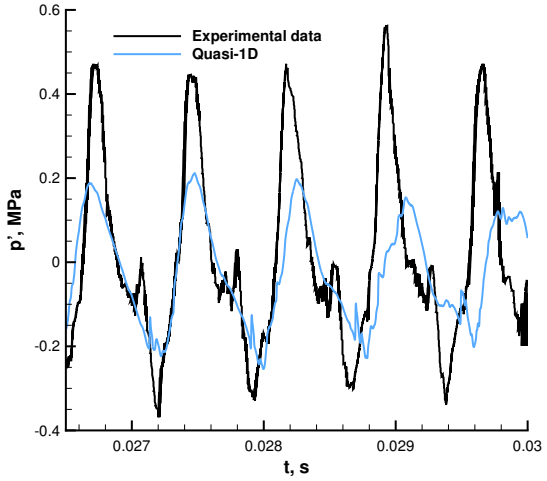

(b) l_{op} = 13.97 cm.

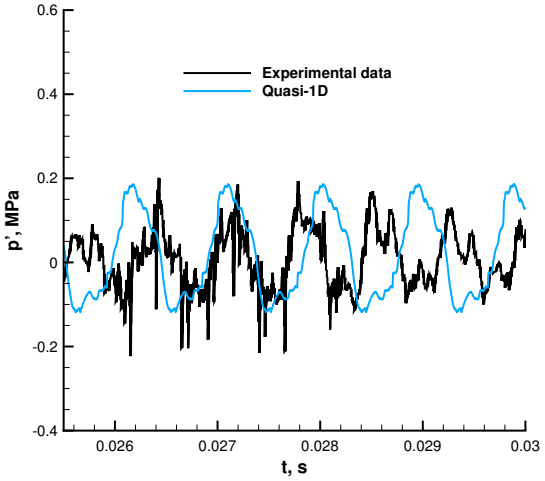

(c) l_{op} = 8.89 cm.

Figure 4: Comparison between obtained limit cycles[7] and experimental data of CVRC.[25,31]

Table 3: Comparison between numerical[7] and experimental[25,31] limit cycle resonant frequencies of CVRC.

	l_{op} = 8.89 cm		l_{op} = 13.97 cm		l_{op} = 19.05 cm	
	Exp	Q-1D	Exp	Q-1D	Exp	Q-1D
f_1, Hz	1379	1075	1324	1287	1260	1297
f_2, Hz	2734	2150	2653	2562	2520	2580
f_3, Hz	3882	3237	3979	3587	3780	3878

DOI: 10.13009/EUCASS2019-617

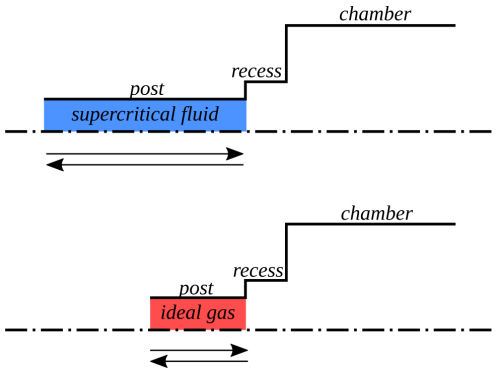

Figure 5: The post length has been recomputed in order to preserve the acoustic characteristic time of the supercritical fluids.

3.2 BKD test-case

BKD engine is an even more interesting test-case to be analyzed since its design parameters are compliant to those of a real life-size upper stage. It is fed by hydrogen and oxygen, both at supercritical pressure and the former at supercritical temperature while the latter at subcritical temperature. Its operative pressure can be increased up to 8 MPa. Such system is affected by transverse combustion instability[10–13] and, as mentioned in Section 3, the aim of the present work is to focus the attention on only one of its injectors, using the presented one-dimensional low-order model. For such a reason, several modeling assumption have been introduced. What is presented in this section is the current state of development of the model aiming to its application to supercritical fluids, and an overview of the critical modeling aspects.

Supercritical fluids would require real gas models whereas at the present status of development the approach can only deal with perfect gases. Therefore, the supercritical fluids have to be replaced with equivalent ideal gases. BKD is operated with oxygen and hydrogen respectively injected at 111 K and 96 K, thus thermally perfect gases O_2 and H_2 have been taken into account, at those temperatures. Accordingly, a modified injector is considered to keep the same acoustic behavior as the real one while retaining the perfect gas assumption. Since real and ideal gases have significantly different acoustic features at that thermodynamic state, in order to match the acoustic characteristic timing of the actual injector, the length of the oxidixer post (L_g) has been recomputed by taking the real gas properties from the National Institute of Standards and Technology (NIST) database[18] and imposing the acoustic time to be preserved

$$\left(\frac{L}{u+a}-\frac{L}{u-a}\right)_r=\left(\frac{L}{u+a}-\frac{L}{u-a}\right)_i \tag{13}$$

where subscript r stands for the real gas features of BKD while i for the ideal gas quantities. The corresponding geometrical model is shown in Figure 5.

As far as the combustion chamber is concerned, since the BKD engine is affected by self-excited combustion instability, its one-dimensional length (L_c) has been chosen in such a way it has the same characteristic acoustic timing of the actual, measured, transverse instability frequency of BKD.

$$L_c=\frac{a}{2f_{1T,BKD}} \tag{14}$$

where $f_{1T,BKD}$ is the experimentally measured resonant frequency. Using such kind of modeling the problem has been reduced to a single dimension and preserves its self-excited nature. BKD geometric and operative parameters, for both the real engine and the equivalent single injector systems with perfect gas, are summarized in Table 4.

The response function formulation needs a slight modification: it has to be recast to consider oxidizer accumulation, rather than fuel. The reason for such need lies in the combustion model. As stated in Section 2 and shown in Eq. (9), the model assumes stoichiometric combustion and produces a stoichiometric equilibrium mixture. Since BKD is a fuel rich system, differently from CVRC, it is easy to figure out that an additional release of fuel mass would produce a major dilution of the mixture which would produce no increase in the instantaneous heat release rate in turn. If the oxidizer is accumulated, on the other hand, the model is able to behave correctly being able to burn a major amount of stoichiometric mixture, in case such event takes place.

DOI: 10.13009/EUCASS2019-617

Table 4: BKD geometrical data and operating conditions for the whole system[10–13] and for the single injector system here designed.

Parameter	**Value**	
	Real system	Single injector
Fuel Mass Flow Rate, kg/s	0.96	0.0229
Fuel Temperature, K	96	200
Oxidizer Mass Flow Rate, kg/s	5.75	0.1369
Oxidizer Temperature, K	111	200
Equivalence Ratio	1.323	1.323
Throat diameter, cm	5	0.77
Combustor length, cm	20	7.63
Combustor diameter, cm	8	1.24
Recess diameter, cm	0.45	0.45
Recess length, cm	0.20	0.20
Oxidizer post diameter, cm	0.36	0.36
Oxidizer post length, l_{op}, cm	7	2.13

3.2.1 Steady state analysis

First of all the steady state is computed turning the response function off. Differently from the case of CVRC, BKD steady state shows a chamber pressure which is lower than the experimental value. In particular the appearing value is 7.23 MPa while the actual average chamber pressure of the real engine is 8 MPa. This is justified by the chamber temperature which is about 450 K lower with respect to the equilibrium adiabatic temperature. The issue lies in the assumption of stoichiometric combustion: chemical equilibrium is nonlinear while the model assumes stoichiometric combustion plus dilution. Such linearization represents a critical aspect of this kind of formulation because it introduces an error especially when dealing with species having significantly different properties with respect to the others, e.g., hydrogen. As a first approximation to fix this issue, the effective acoustic chamber length (L_c, see Eq. (14)) has been recomputed using the resulting lower temperature of 3111 K, rather than the adiabatic flame temperature of 3579 K.

3.2.2 Preliminary unsteady operations results

The unsteady analyses have been carried out analogously to the CVRC test-case, with one difference: the response function calibration parameter σ needs an upper limit now that accumulation of oxidizer is being considered. It is reasonable to believe that also the heavier oxidizer can be accumulated into vortexes, at the recess location, but it is not possible to assume that the oxidizer mass flow rate gets completely disrupted. For such reason the maximum mass flow rate allowed to be instantaneously accumulated, and then released, is constrained to the specific amount allowing the flow mixture to reach the stoichiometric value locally, i.e. the value allowing for the maximum heat to be released during combustion.

Results are shown in Figure 6. The BKD single injector system shows self-excited instability and a limit cycle is reached. Its dominant frequency is 39.1 kHz, while the resonant frequency of the BKD engine system is ∼10 kHz. The reason of the fact that their ratio is that close to four lies in the fact that the system oscillates on the fourth chamber longitudinal resonant frequency, as shown by the unsteady pressure field in Figure 6c. Such phenomenon tells that a feedback loop exists, even if it is around the wrong harmonic. Figure 6b shows the instantaneous oxidizer mass flow rate being affected by accumulation or release, at the recess location during limit cycle.

The reasons of such kind of coupling still need to be further investigated. One reason could lie in the fact that, as previously mentioned, the 1T resonant frequency of the BKD engine system has been used to determine the chamber length. This is a quite strong assumption given the fact that such frequency is the outcome of a fully coupled strongly nonlinear operating system. Switching from a nonlinear system to another it is not straightforward that those linearized acoustic lengths should be comparable.

4. Conclusions

A recently introduced low-order model for thermoacoustic combustion instability has been used in this work to compare results which can be obtained for quite different test-cases. The coupling between pressure oscillations and propellant

DOI: 10.13009/EUCASS2019-617

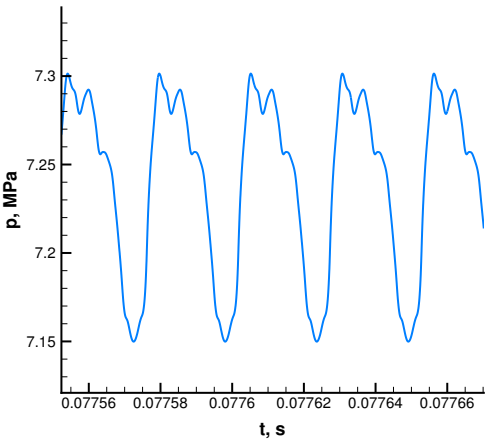

(a) Pressure signal sampled at the chamber aft-end.

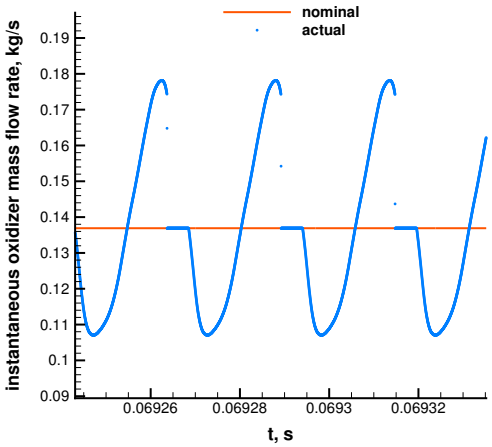

(b) Instantaneous oxidizer mass flow rate being accumulated or released at recess location.

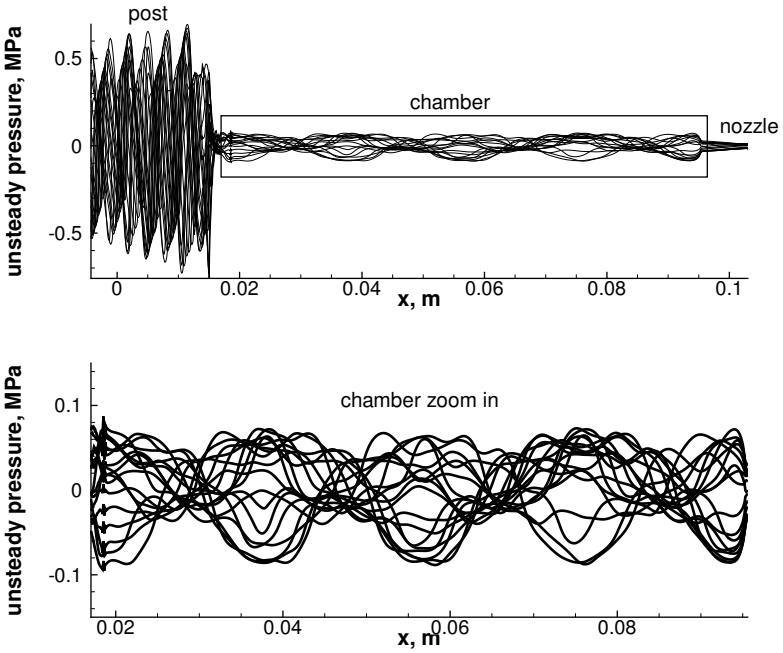

(c) Pressure trends in space, over time. Snapshots show the typical shape of a 4L mode, in the chamber.

Figure 6: The resulting BKD limit cycle.

DOI: 10.13009/EUCASS2019-617

injection has been applied to two different test-cases: the former is the CVRC engine, fed by gaseous propellant in oxidizer rich proportion, while the latter is BKD engine, fed by supercritical fuel and oxidizer in fuel rich proportion.

The CVRC application showed that the model works quite well, when dealing with hot gases. CVRC limit cycle is recovered for each of the three simulated geometrical configurations, within a certain threshold. An important outcome is that the shape of the experimental signal is well reproduced, meaning that the main gasdynamics events are captured by the model.

The BKD application is much more challenging both for the fact that it operates supercritical propellant and because its geometry has been reduced to an equivalent one-dimensional domain approximating the engine transverse instability features. This preliminary work aimed to reproduce the instability of a single load point. Also in this case, instability arises. The resonant frequency is four times the actual one and the reason is that the reduced single injector system fluctuates on its fourth longitudinal resonant frequency. Based on these preliminary results the continuation of the study aims to extend modeling to real fluids and to improve the modeling of the mixture properties, in conditions different from nominal, due to dilution with fuel or oxidizer during the mass flow ratio oscillation phases.

References

[1] C. A. Armitage, R. Balachandran, E. Mastorakos, and R. S. Cant. Investigation of the nonlianear response of turbulent premixed flames to imposed inlet velocity oscillations. *Combustion and Flame, Vol. 146, pp. 419-436*, 2006.

[2] L. T. W Chong, S. Bomberg, A. Ulhaq, T. Komarek, and W. Polifke. Comparative validation study on identification of premixed flame transfer function. *Journal of Engineering for Gas Turbines and Power, Volume 134*, 2012.

[3] L. T. W Chong, T. Komarek, R. Kaess, S. Foller, and W. Polifke. Identification of flame transfer function from les of a premixed swirl burner. 2010. ASME Turbo Expo 2010: Power for Land, Sea and Air, June 14-18, Glasgow, UK.

[4] L. Crocco and S.I. Cheng. *Theory of Combustion Instability in Liquid Propellant Rocket Motors*. Butterworths Scientific Publication, 1956.

[5] F. E. C. Culick and V. Yang. Combustion instabilities in liquid rockets. *Liquid Rocket Engine Combustion Instability, Vol. 169, AIAA, pp.3-37*, 1995.

[6] M. L. Frezzotti, S. D'Alessandro, B. Favini, and F. Nasuti. Numerical issues in modeling combustion instability by quasi-1d euler equations. *International Journal of Spray and Combustion Dynamics*, 0(0):1756827717711015, 2017.

[7] M L Frezzotti, S D'Alessandro, B Favini, and F Nasuti. Driving mechanisms in low order modeling of longitudinal combustion instability. American Institute of Aeronautics and Astronautics, 2018. AIAA Propulsion and Energy Forum, Cincinnati, OH, USA, 9–11 July.

[8] M. L. Frezzotti, F. Nasuti, C. Huang, C. L. Merkle, and W. E. Anderson. Quasi-1d modeling of heat release for the study of longitudinal combustion instability. *Aerospace Science and Technology*, pages 261–270, February 2018. doi: 10.1016/j.ast.2018.02.001.

[9] R. Garby, L. Selle, and T. Poinsot. Large-eddy simulation of combustion instabilities in a variable-length combustor. *Comptes Rendus Mécanique*, 341(1-2):220–229, January 2013. doi:10.1016/j.crme.2012.10.020.

[10] S. Gröning, J. S. Hardi, D. Suslov, and M. Oschwald. Analysis of phase shift between oscillations of pressure and flame radiation intensity of self-excited combustion instabilities. 6th European Conference for Aeronautics and Space Sciences, June 29th - July 3rd 2015, Krakow, Poland.

[11] S. Gröning, J.S. Hardi, D. Suslov, M. Oschwald, and E.S. Kim. Injector-driven combustion instabilities in a hydrogen/oxygen rocket combustor. *Journal of Propulsion and Power*, 32(3):560–573, May-June 2016. doi=:10.2514/1.B35768.

[12] S. Gröning, D. Suslov, J. S. Hardi, and M. Oschwald. Influence of hydrogen temperature on the acoustics of a rocket engine combustion chamber operated with lox/h2 at representative conditions. Space Propulsion Conference, May 2014, Cologne, Germany.

DOI: 10.13009/EUCASS2019-617

[13] S. Gröning, D. Suslov, M. Oschwald, and T. Sattelmayer. Stability behaviour of a cylindrical rocket engine combustion chamber operated with liquid hydrogen and liquid oxygen. 5th European Conference for Aeronautics and Space Sciences, July 2013, Munich, Germany.

[14] M. E. Harvazinski, W. E. Anderson, and C. L. Merkle. Analysis of self-excited combustion instability using two- and three-dimensional simulations. *Journal of Propulsion and Power, Vol. 29, pp. 396-409*, 2013.

[15] M. E. Harvazinski, C. Huang, V. Sankaran, T. W. Feldman, W. E. Anderson, C. L. Merkle, and D. G. Talley. Coupling between hydrodynamics, acoustics and heat release in a self-excited unstable combustor. *Physics of Fluids, Vol. 27, 045102*, 2015.

[16] M. E. Harvazinski, D. G. Talley, and V. Sankaran. Influence of boundary condition treatment on longitudinal mode combustion instability predictions. 2013. 49th AIAA/ASME/SAE/ASEE Joint Propulsion Conference, July, San Jose, CA.

[17] H. J. Krediet, C. H. Beck, W. Krebs, S. Schimek, C. O. Paschereit, and J. B. W. Kok. Identification of the flame describing function of a premixed swirl flame from les. *Combustion Science and Technology, vol. 184, pp. 888-900*, 2012.

[18] Eds. P.J. Linstrom and W.G. Mallard. *NIST Chemistry WebBook, NIST Standard Reference Database Number 69*. National Institute of Standards and Technology.

[19] K. I. Matveev. Vortex-acoustic instability in chambers with mean flow and heat release. *Electronic Journal "Technical Acoustics"*, 2004.

[20] B. J. McBride and S. Gordon. Computer program for calculation of complex chemical equilibrium compositions and applications. Technical Report 1311, 1994. NASA Reference Publication.

[21] J. C. Oefelein and V. Yang. Comprehensive review of liquid-propellant combustion instabilities in f-1 engines. *Journal of Propulsion and Power, Vol. 9, No. 5, September-October*, 1993.

[22] L. O'Hara, Y. Yu, R. J. Smith, W. E. Anderson, and C. Merkle. Investigations to an unsteady heat release model applied to an unstable liquid rocket combustor. 2009. 45th AIAA/ASME/SAE/ASEE Joint Propulsion Conference & Exhibit, 2-5 August, Denver, Colorado.

[23] P. P. Popov, A. Sideris, and W. A. Sirignano. Stochastic modelling of transverse wave instability in a liquid-propellant rocket engine. *Journal of Fluid Mechanics*, 745:62–91, April 2014. doi:10.1017/jfm.2014.96.

[24] J. E. Portillo, J. C. Sisco, Y. Yu, and W. E. Anderson. Application of generalized instability model to a longitudinal mode combustion instability. 2007. 43th AIAA/ASME/SAE/ASEE Joint Propulsion Conference & Exhibit, 8-11 July, Cincinnati, OH.

[25] S. V. Sardeshmukh, W. E. Anderson, M. E. Harvazinski, and V. Sankaran. Prediction of combustion instability with detailed chemical kinetics. 53th AIAA Aerospace Science Meeting, January 2015, Kissimmee, FL.

[26] L. Selle, M. Blouquin, M. Thèron, L.H. Dorey, M. Shmid, and W. E. Anderson. Prediction and analysis of combustion instability in a model rocket engine. *Journal of Propulsion and Power, Vol. 30, No. 4*, 2014.

[27] C. F. Silva, T. Emmert, S. Jaensch, and W. Polifke. Numerical study on intrinsic thermoacoustic instability of a laminar premixed flame. *Combustion and Flame, Vol. 162, pp. 3370-3378*, 2015.

[28] W. A. Sirignano and P. P. Popov. Two-dimensional model for liquid-rocket transverse combustion instability. *AIAA Journal, Vol. 51, No. 12, pp. 2919-2934*, 2013.

[29] J. C. Sisco, J. E. Portillo, Y. C. Yu, and W. E. Anderson. Non-linear characteristic of longitudinal instabilities in a model rocket combustor. 2007. 43rd AIAA/ASME/SAE/ASEE Joint Propulsion Conference & Exhibit, 8-11 July, Cincinnati, OH.

[30] R. Smith, M. Ellis, G. Xia, V. Sankaran, W. Anderson, and C. L. Merkle. Computational investigation of acoustics and instabilities in a longitudinal-mode rocket combustor. *AIAA Journal, Vol. 46, No. 11, November*, 2008.

[31] S. Srinivasan, R. Ranjan, and S. Menon. Flame dynamics during combustion instability in a high-pressure, shear-coaxial injector combustor. *Flow, Turbulence and Combustion, Vol.94, pp. 237-262*, 2015.

DOI: 10.13009/EUCASS2019-617

[32] P. Tudisco, R. Ranjan, S. Menon, S. Jaensch, and W. Polifke. Application of the time-domain impedance boundary condition to large-eddy simulation of combustion instability in a shear-coaxial high pressure combustor. *Flow, Turbulence and Combustion*, 99(1):1–23, March 2017. doi: 10.1007/s10494-017-9804-3.

[33] A. Urbano, L. Selle, G. Staffelbach, B. Cuenot, T. Schmitt, S. Ducruix, and S. Candel. Exploration of combustion instability triggering using large eddy simulation of a multiple injector liquid rocket engine. *Combustion and Flame, Vol. 169, pp. 129-140*, 2016.

[34] B. Varoquiè, J. P. Lègier, F. Lacas, D. Veynante, and T. Poinsot. Experimental analysis and large eddy simulation to determine the response of non premixed flame submitted to acoustic forcing. 29th International Symposium on Combustion, July 2012.

[35] M. Wierman, N. Nugent, and W. E. Anderson. Combustion response of a lox/lch4 element to tranverse instabilities. AIAA Paper 2011-5549, July 2011. 47th AIAA/SAE/ASEE Joint Propulsion Conference, San Diego, CA, doi:10.2514/6.2011-5548.

[36] Y. C. Yu. *Experimental and analytical Investigations of Longitudinal Combustion Instability in a Continuously Variable Resonance Combustor (CVRC)*. PhD thesis, Purdue University, School of Aeronautics and Astronautics, 2009.

[37] Y. C. Yu, S. M. Koeglmeier, J. C. Sisco, R. J. Smith, and W. E. Anderson. Combustion instability of gaseous fuels in a continuously variable resonance chamber (cvrc). 2008. 44th AIAA/ASME/SAE/ASEE Joint Propulsion Conference & Exhibit, July, Hartford, CT.

[38] Y. C. Yu, L. O'Hara, J. C. Sisco, and W. E. Anderson. Examination of mode shapes in an unstable model rocket combustor. 2009. 47th AIAA Aerospace Sciences Meeting Including the New Horizons Forum and Aerospace Expositions, 5-8 January, Orlando, Florida.

[39] Y. C. Yu, J. C. Sisco, S. Rosen, A. Madhav, and W. E. Anderson. Spontaneous longitudinal combustion instability in a continuously-variable resonance combustor. *Journal of Propulsion and Power, Vol. 28, pp. 876-887*, 2012.

[40] Y. C. Yu, J. C. Sisco, V. Sankaran, and W. E. Anderson. Effects of mean flow, entropy waves and boundary conditions on longitudinal combustion instability. *Combustion Science and Technology, vol. 182, pp. 739-776*, 2010.